Journal of Catalysis 270 (2010) 206–212

Contents lists available at ScienceDirect

Journal of Catalysis

journal homepage: www.elsevier.com/locate/jcat

Layered and nanosheet tantalum molybdate as strong solid acid catalysts

Caio Tagusagawa [a], Atsushi Takagaki [b], Kazuhiro Takanabe [a], Kohki Ebitani [b], Shigenobu Hayashi [c], Kazunari Domen [a,*]

[a] Department of Chemical System Engineering, School of Engineering, The University of Tokyo, 7-3-1, Hongo, Bunkyo-ku, Tokyo 113-7656, Japan
[b] School of Materials Science, Japan Advanced Institute of Science and Technology (JAIST), 1-1 Asahidai, Nomi, Ishikawa 923-1292, Japan
[c] Research Institute of Instrumentation Frontier, National Institute of Advanced Industrial Science and Technology (AIST), Central 5, 1-1-1 Higashi, Tsukuba, Ibaraki 305-8565, Japan

ARTICLE INFO

Article history:
Received 28 October 2009
Revised 16 December 2009
Accepted 25 December 2009
Available online 27 January 2010

Keywords:
Solid acid
Layered metal oxides
Nanosheets
Friedel–Crafts alkylation
Hydrolysis
NH_3 temperature-programmed desorption
^{31}P magic-angle spinning nuclear magnetic resonance spectroscopy

ABSTRACT

Layered and nanosheet aggregates of $HTaMoO_6$ were examined as solid acid catalysts. The $HTaMoO_6$ aggregated nanosheets were formed by soft chemical processing of layered $HTaMoO_6$ using tetra (*n*-butylammonium) hydroxide. The catalytic activity and acid properties of the $HTaMoO_6$ compounds were compared with those of layered $HNbMoO_6$ and a range of conventional solid acids. The catalytic activity of $HTaMoO_6$ for Friedel–Crafts alkylation with benzyl alcohol, hydrolysis of disaccharides, and esterification of acetic acid and lactic acid increased after exfoliation and aggregation, consistent with the acid strengths determined by NH_3 temperature-programmed desorption and ^{31}P magic-angle spinning nuclear magnetic resonance spectroscopy measurements. $HTaMoO_6$ nanosheets possess additional strong acid sites on the oxide formed by exposure of a single layer, along with strong acid sites within the interlayer of the layered aggregate structure, resulting in higher acid catalytic activity than that of the original layered oxide.

© 2009 Elsevier Inc. All rights reserved.

1. Introduction

The development of environment-friendly chemical processes is important to the chemical industry [1,2]. The present authors have been developing solid acid catalysts to replace liquid acid catalysts such as sulfuric acid and fluoric acid. Unlike liquid acids, solid acids (clay minerals [3–5], zeolites [6–8], Cs-heteropoly acids [9–11], sulfated zirconia [12–14], ion-exchange resins [15], and sulfonated-carbon materials [16,17]) are reusable for heterogeneous reactions (liquid/solid, gas/solid), simplifying the separation of products and minimizing the formation of liquid waste that requires neutralization [18,19].

H^+-exchanged forms of cation-exchangeable transition metal layered oxides, in which H^+ ions are located between two-dimensional (2D) transition metal oxide anion sheets, are potentially useful as strong solid acids. However, because the high charge density of the oxide sheets prevents reactants from penetrating into the interlayer region, unmodified layered transition metal oxides have been generally ineffective as solid acid catalysts. To overcome this disadvantage, previous studies have revealed that layered metal oxides can be applied as solid acid catalysts after exfoliation of the layers and aggregation of the formed nanosheets [20–24]. Exfoliation of cation-exchangeable layered metal oxides such as $HTiNbO_5$, HTi_2NbO_7, $HTiTaO_5$, HNb_3O_8, $HNbWO_6$, and $HTaWO_6$ in aqueous solution affords colloidal single-crystal metal oxide sheets that precipitate under acidic conditions to form aggregates of nanosheets. These nanosheet aggregates possess a high specific surface area (ca. 100 $m^2\,g^{-1}$ for $HTiNbO_5$, HTi_2NbO_7, $HTiTaO_5$, and HNb_3O_8, and ca. 50 $m^2\,g^{-1}$ for $HNbWO_6$ and $HTaWO_6$) and exhibit a high catalytic activity for acid-catalyzed reactions such as Friedel–Crafts alkylation [22,24], the esterification of acetic acid [20–22], the hydrolysis of ethyl acetate [20–22], and the dehydration of D-xylose [23].

Recently, we found that protonated, layered niobium molybdate ($HNbMoO_6$) functions as a solid acid catalyst without modification due to the facility of intercalation of reactants during several acid-catalyzed reactions, such as Friedel–Crafts alkylation, esterification of lactic acid, hydration of 2,3-dimethyl-2-butene, acetalization of cyclohexanone, and hydrolysis of disaccharides [25–28]. Layered $HNbMoO_6$ exhibited a considerably high reaction rates for these reactions, exceeding those of ion-exchange resins, zeolites, and niobic acids [25]. For instance, the turnover rate of $HNbMoO_6$ for the alkylation of anisole was over three times higher than that of Nafion NR50 [25].

In the present study, layered metal oxide $HTaMoO_6$ and its aggregated nanosheets were examined as novel solid acid catalysts.

* Corresponding author. Fax: +81 3 5841 8838.
E-mail address: domen@chemsys.t.u-tokyo.ac.jp (K. Domen).

0021-9517/$ - see front matter © 2009 Elsevier Inc. All rights reserved.
doi:10.1016/j.jcat.2009.12.019

Our previous studies demonstrated that aggregated nanosheets based on tantalum, such as $HTiTaO_5$ and $HTaWO_6$, possess higher acid strength, resulting in higher performance in acid-catalyzed reactions than that of these niobium-substituted oxides ($HTiNbO_5$ and $HNbWO_6$) [21,24]. Substitution of Ta for Nb was found to be very effective in generating strong acid sites on nanosheets. $HTaWO_6$ nanosheets exhibited remarkable activity for Friedel–Crafts alkylation of anisole with benzyl alcohol, giving a yield six times higher than that for $HNbWO_6$ nanosheets. These strong acid sites are formed on the surface of nanosheets.

In contrast, acid catalytic activity of layered $HNbMoO_6$ is attributed to the intercalation of substrate within the interlayer with strong acidity [25–28]. The acid sites are located in the interlayer gallery much different from the acid sites of nanosheets, confirmed by ^{31}P magic-angle spinning nuclear magnetic resonance (MAS-NMR) and NH_3 temperature-programmed desorption (NH_3-TPD) study. This efficient acid catalysis to utilize interlayer space was observed only for the case of layered $HNbMoO_6$. Therefore, layered $HTaMoO_6$, which consists of an isomorphous structure of $HNbMoO_6$, was tested in an attempt to obtain a more effective solid acid than $HNbMoO_6$. The present study is the first successful example of layered Ta-based oxide to exhibit considerable catalytic activity for several acid-catalyzed reactions. Nanosheet catalysts were prepared from the lithium form of the layered metal oxide, $LiTaMoO_6$ (Fig. 1) by proton exchange and subsequent exfoliation using tetra(*n*-butylammonium) hydroxide (TBA^+OH^-) [29–34]. Layered $HTaMoO_6$ was compared with its aggregate nanosheets and layered $HNbMoO_6$ to investigate the effects of exfoliation on the acid properties of $HTaMoO_6$ and the effects of replacing the metal cation Ta^{5+} with Nb^{5+}. The acid properties of these solid acids were evaluated by NH_3-TPD and ^{31}P MAS NMR spectroscopy. The acid catalytic activity of $HTaMoO_6$ solid acids was examined during liquid-phase Friedel–Crafts alkylation of anisole and toluene, esterification of acetic and lactic acid, and hydrolysis of disaccharides, and the results were compared with those of conventional solid acids.

2. Experimental

2.1. Preparation of layered $HTaMoO_6$ and nanosheet aggregates

Layered $HTaMoO_6$ was prepared by proton exchange of precursor $LiTaMoO_6$, which was obtained by calcination of a stoichiometric mixture of Li_2CO_3 (99.95% Kanto), Ta_2O_5 (99.9% Kojundo), and MoO_3 (99.5% Kanto) at 873 K for 24 h with one intermediate grinding [31,32]. The proton-exchange reaction was performed by shaking 2.0 g of the lithium form in 150 mL of 1 M nitric acid (Wako) solution at room temperature for 2 weeks, exchanging the acid solution twice over that period. The product was then washed with distilled water and dried in air at 343 K. Layered $HNbMoO_6$ was prepared using the same procedure, but with $LiNbMoO_6$ as the precursor [25–29].

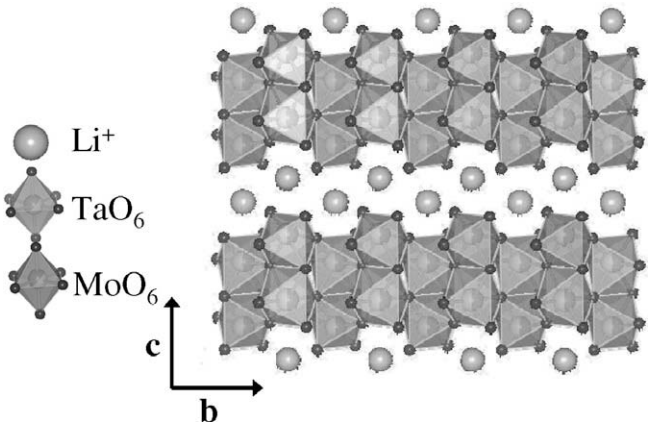

Fig. 1. A schematic structure of layered $LiTaMoO_6$.

The nanosheets constituting the layered oxides ($TaMoO_6^-$ nanosheets) were prepared by adding 15 wt% tetra(*n*-butylammonium) hydroxide (TBA^+OH^-) solution (10% Wako) to 150 mL of distilled water containing 2.0 g of the protonated compound. The TBA^+OH^- solution was added to the suspension until the pH reached 9.5–10.0, and the resultant solution was shaken for 2 weeks. The insertion of voluminous and hydrophilic TBA^+ cations expanded and hydrated the interlayer spaces, resulting in the exfoliation of metal oxide sheets. After shaking, the suspension was centrifuged, and the supernatant solution containing the dispersed nanosheets was collected. The addition of HNO_3 aqueous solution (0.1 M, 30 mL) to 150 mL of the nanosheet solution resulted in immediate aggregation of the nanosheets as a precipitate. The aggregated nanosheet samples were then rinsed three times with 150 mL of 0.1 M HNO_3 aqueous solution to remove TBA^+, and then with 150 mL of distilled water to remove HNO_3, the complete removal of which was confirmed by elemental analysis.

The present study uses excess amount of HNO_3 for the production of $HTaMoO_6$ samples in order to understand the acid catalysis of them clearly. It is possible to reduce the amount of HNO_3 used for ion-exchange and aggregation processes to at least one third.

2.2. Characterization

Samples were characterized by X-ray diffraction (XRD; RINT-UltimaIII, Rigaku), scanning electron microscopy (SEM; S-4700, Hitachi), and N_2 desorption (BEL Japan, BELSORP-miniII). The acid properties of the samples were determined by NH_3 temperature-programmed desorption using a TPD-1-AT instrument (BEL Japan) equipped with a quadrupole mass spectrometer. In the TPD measurements, a 20 mg sample was heated at 423 K for 1 h under helium flow, exposed to NH_3 at 373 K for adsorption, exposed to He at 373 K for 1 h to remove excess NH_3, and finally heated at 5 K min^{-1}.

^{31}P MAS NMR spectra were measured at room temperature using Bruker ASX400 spectrometer at Larmor frequency of 162.0 MHz. Bruker MAS probehead was used in combination with a 4-mm zirconia rotor operated at a sample spin rate of 8 or 10 kHz. The ^{31}P NMR chemical shift was referenced to 85% H_3PO_4 (at 0.0 ppm) by setting the signal of $(NH_4)_2HPO_4$ at 1.33 ppm. For ^{31}P NMR, trimethylphosphine oxide (TMPO) (Alfa Aesar) was employed as a probe molecule. TMPO-adsorbed samples were prepared by evacuated dehydration at 423 K for 1 h followed by immersion in tetrahydrofuran (THF) (99.5% nacalai tesque) solution containing TMPO (0.333 mol L^{-1} THF solution) at room temperature for 2 days in a glovebox under argon. After evacuation to remove the THF solvent, the samples were packed in a rotor housed in a glovebox under N_2.

2.3. Acid-catalyzed reaction

The acid catalytic activity of layered $HTaMoO_6$ and aggregated nanosheets, without pretreatment, was determined through Friedel–Crafts alkylation, esterification, and hydrolysis.

Friedel–Crafts alkylation of anisole (99% Wako) or toluene (99.5% Kanto) with benzyl alcohol (99% Kanto) was performed using 0.2 g of the catalyst, 100 mmol of anisole or toluene, 10 mmol of benzyl alcohol, and *n*-decane (99% Wako) or octane (98% Wako) as an internal standard. The reaction vessel was placed in an oil bath maintained at 353–373 K for the duration of the 2–4-h reaction. The products (benzylanisole, benzyltoluene,

and dibenzyl ether) were analyzed by a gas chromatography equipped with a flame ionization detector (GC-2014, Shimadzu) using a capillary column (J&W Scientific DB-FFAP). The activities of layered $HNbMoO_6$, ion-exchange resins (Amberlyst-15 and Nafion NR50), and H-type zeolite (H-Beta – SiO_2/Al_2O_3 = 25, JRC-Z-HB25 supplied from Catalysis Society of Japan (Japan Reference Catalyst)), pretreated at 423 K in vacuum, were also determined for comparison.

Esterification of acetic acid (99.7% Wako) or lactic acid (85–92% Wako) was performed using 0.2 g of the catalyst, 0.10 mol of acetic acid or 0.088 mol of lactic acid and 1 mol of ethanol (99.5% Kanto). The reaction vessel was placed in an oil bath maintained at 343 K for the duration of the 2–4-h reaction. The product was examined by the same flame ionization gas chromatography as above, using 2-butanol (99% Wako) as an external standard.

Hydrolysis of disaccharides (sucrose or cellobiose) was carried out at 353 or 368 K using 0.1 g of the catalyst, 0.5 g (1.46 mmol) of sucrose (Wako) or cellobiose (Kanto), and 5–10 mL of water in a 4-h reaction. The products for hydrolysis of disaccharides were analyzed by high-performance liquid chromatography (HPLC; LC-2000 plus, JASCO) using Shodex Asahipak NH2P-50.

3. Results and discussion

3.1. Structures of layered metal oxides and aggregated nanosheets

Layered $HTaMoO_6$ has the same trirutile structure as layered $HNbMoO_6$. Protons and water are embraced by two-dimensional sheets comprised of ordered-located TaO_6 and MoO_6 octahedra with small disorder between TaO_6 and MoO_6 [31–32]. The XRD patterns for the layered $LiTaMoO_6$, $HTaMoO_6{\cdot}nH_2O$, and the aggregated nanosheet are shown in Fig. 2. The interlayer space of $LiTaMoO_6$ increased after proton-exchange formed $HTaMoO_6{\cdot}nH_2O$, with n estimated to be 1.35 according to thermogravimetry (TG). An impurity phase ascribed to $LiTaO_3$ was observed at 23° in both Li and H forms of layered metal oxides. The XRD pattern for the $HTaMoO_6$ nanosheet precipitate retained a strong diffraction peak at low angle ($2\theta < 10°$), indicating that the exfoliated nanosheets ($TaMoO_6^-$) aggregated randomly in the layered structure with preservation of in-plane diffraction peaks ((1 1 0) and (2 0 0)) and the total absence of other peaks ((1 1 2), (1 0 7), and (1 0 9)).

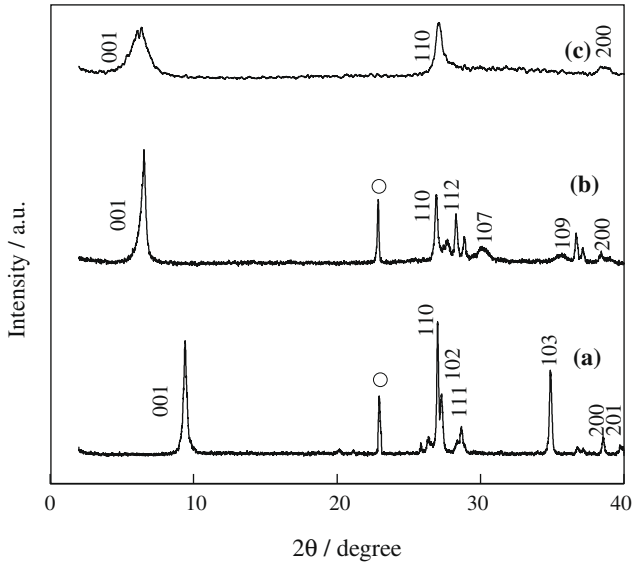

Fig. 2. XRD patterns for (a) layered $LiTaMoO_6$, (b) layered $HTaMoO_6{\cdot}nH_2O$, and (c) $HTaMoO_6$ nanosheet aggregate (○ = $LiTaO_3$ as impurity).

SEM images of layered $LiTaMoO_6$, layered $HTaMoO_6$, and $HTaMoO_6$ nanosheets are shown in Fig. 3. The as-prepared layered metal oxides consisted of tabular particles, 3–20 μm in size, with a Brunauer–Emmet–Teller (BET) surface of 1–2 $m^2\ g^{-1}$. The SEM image of the aggregated-nanosheet precipitates indicates that the addition of acid (H^+) resulted in the aggregation of nanosheets into a layered structure, with the expected composition (confirmed by energy-dispersed X-ray spectroscopy). The BET surface area of the $HTaMoO_6$ nanosheet was 23 $m^2\ g^{-1}$, comparable to that of $HNbMoO_6$ nanosheets, 14 $m^2\ g^{-1}$ [26,27]. This result was much lower than that of other aggregated-nanosheet metal oxides, such as $HTiNbO_5$ and HNb_3O_8, which typically have surface areas exceeding 100 $m^2\ g^{-1}$ [26–30]. This indicates that most of the exfoliated [$MMoO_6$] sheets (M = Nb or Ta) were restacked into the original layered structure, probably due to the high charge density of the two-dimensional sheets.

3.2. NH_3-TPD

The NH_3-TPD (m/e = 16, temperature increasing rate; 5 K min^{-1}) results for the layered and nanosheet $HTaMoO_6$ used to determine the acid strength from the desorption temperature of NH_3 are shown in Fig. 4. The result for layered $HNbMoO_6$ is shown for comparison. The NH_3-TPD profile for layered $HTaMoO_6$ exhibits two distinct peaks, at 436 and 678 K. The position of latter peak is higher than that of layered $HNbMoO_6$ at 636 K. The profile for $HTaMoO_6$ nanosheets contains three distinct peaks, at 437, 562, and 711 K. The high-temperature peaks (678, 636, and 711 K) were close to the NH_3 desorption peaks obtained for layered $HNbWO_6$ (652 K) and $HTaWO_6$ (668 K [24]), which are attributable to strong acid sites formed in the interlayer of layered structures. The formation of the new peak at 562 K for $HTaMoO_6$ nanosheets and the difference in desorption temperatures between layered and nanosheet $HTaMoO_6$ can be attributed to the structural change induced by the exfoliation–aggregation process. This process exposes intrinsic OH groups on individual two-dimensional sheets, resulting in the formation of strong acid sites on the nanosheets, which appear as a peak at 562 K for NH_3-TPD. Similar distinctive nanosheet peaks have been observed for other metal oxide nanosheets in the same region (535–560 K [24]). And the random aggregation of two-dimensional sheets with intrinsic OH groups re-aggregated in layered structures, with high desorption peak at 711 K. The increase on desorption temperature should be caused by the randomly aggregated layered structures. The randomly aggregated structure should have restricted the diffusion of NH_3 and increased the contacts with acid sites, helping the re-adsorption of NH_3 at the acid sites, elevating the desorption temperature.

3.3. ^{31}P MAS NMR

The acid properties of layered and nanosheet $HTaMoO_6$ were also evaluated by ^{31}P MAS NMR using TMPO as a probe molecule, and compared with layered $HNbMoO_6$ (Fig. 5). As the ^{31}P chemical shifts of protonated TMPO (i.e., $TMPOH^+$) tend to move downfield, higher chemical shifts indicate higher protonic acid strength.

A total of 12.5 mol%- or 50 mol%-introduced TMPO (mol TMPO per 100 mol of solid acid) was adsorbed onto layered $HTaMoO_6$ and nanosheet $HTaMoO_6$. Both 50 mol% TMPO-adsorbed samples (Fig. 5b and d) displayed a sharp peak at 41–42 ppm assigned to unreacted TMPO [35]. The appearance of the 41–42-ppm peak indicates that excess TMPO was introduced to these samples, and that all acid sites in these samples were converted. The acid densities determined on the basis of TMPO adsorption were 1.25 mmol g^{-1} for layered $HTaMoO_6$ and 1.00 mmol g^{-1} for $HTaMoO_6$ nanosheets. The acid density measured at aggregated nanosheets is lower than that of layered $HTaMoO_6$ due to random

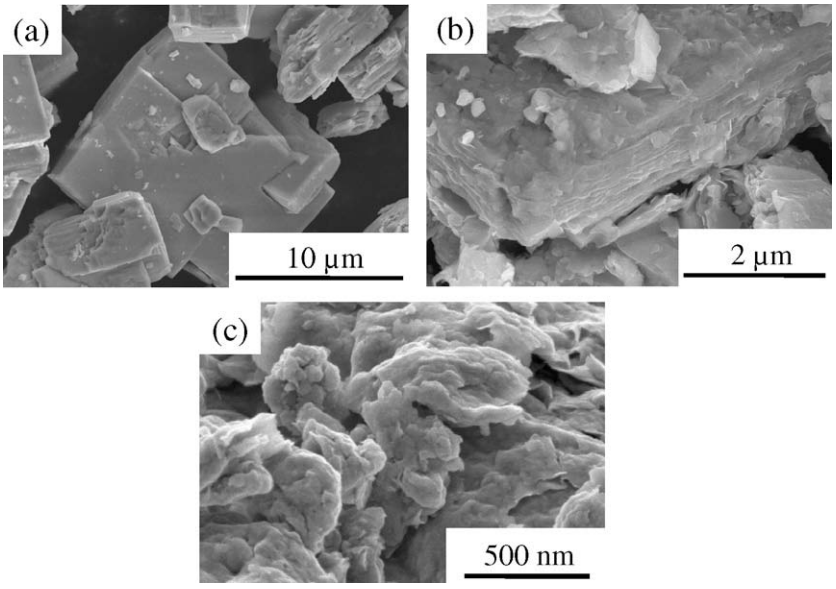

Fig. 3. SEM images of (a) layered $LiTaMoO_6$, (b) layered $HTaMoO_6$, and (c) $HTaMoO_6$ nanosheet aggregate.

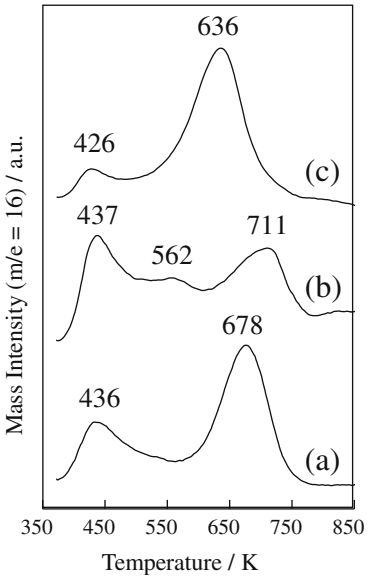

Fig. 4. NH_3-TPD ($m/e = 16$, 5 K min^{-1}) curves for (a) layered $HTaMoO_6$, (b) $HTaMoO_6$ nanosheet aggregate, and (c) layered $HNbMoO_6$.

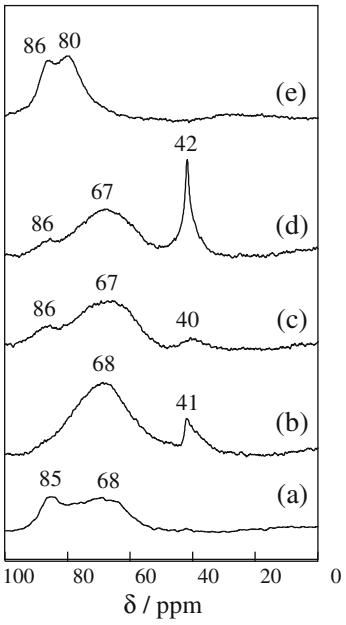

Fig. 5. ^{31}P MAS NMR spectra for TMPO-adsorbed (mol TMPO per 100 mol of solid acid) layered $HTaMoO_6$ after exposure to (a) 12.5 mol% or (b) 50 mol%, $HTaMoO_6$ nanosheets after exposure to (c) 12.5 mol% or (d) 50 mol%, and layered $HNbMoO_6$ after exposure to (e) 22.5 mol% measured at room temperature. The spin rate of the sample was 10 kHz for $HTaMoO_6$ and 8 kHz for $HNbMoO_6$.

aggregation of sheets, which limited the accesses on some hidden nanosheets [24,28].

The 12.5 mol% TMPO-adsorbed samples displayed two main peaks, a very strong acid site at 85–86 ppm and a strong acid site at 67–68 ppm. The peak positions indicate that the acid sites of $HTaMoO_6$ are stronger than those of both H-type zeolites (65 ppm for HY [35], 78 ppm for H-Beta [36]) and ion-exchange resin (81 ppm for Amberlyst-15) and are comparable in strength to those of strongly acidic zeolites (86 ppm for HZSM-5 [37] and HMOR [36]). The result for layered $HNbMoO_6$ is also shown in Fig. 5 and indicates that the peak position of the strong acid sites in $HTaMoO_6$ was comparable to that of $HNbMoO_6$.

Previous studies of layered $HNbMoO_6$ revealed that TMPO as a weak base was intercalated within the interlayer of $HNbMoO_6$, and the peak position of ^{31}P NMR was shifted according to the amount of introduced TMPO [28]. XRD and ^{31}P NMR measurements indicated that a small amount of TMPO formed a monolayer configuration within the interlayer with a strong acidity when a peak ca. 85 ppm was observed in the ^{31}P NMR spectrum. Increased introduction of TMPO led to a bilayer configuration with a peak appearing at ca. 68 ppm in the ^{31}P NMR. This indicates that the TMPO, which was embraced by both sides of the metal oxide sheets in the layered structure, was subjected to their very strong acidity (85 ppm), but TMPO that interacted with only a single metal oxide sheet was subjected to a less-strong acidity (68 ppm).

Note that the peak observed at 85 ppm in the 12.5 mol% TMPO-adsorbed layered $HTaMoO_6$ sample was not observed in the 50 mol% TMPO-adsorbed layered $HTaMoO_6$ sample. The shifts in $HTaMoO_6$ were most likely caused by saturation of the interlayer

by TMPO, resulting in a transition from the monolayer structure (85 ppm) to the bilayer structure (67 ppm). For aggregated nanosheets, however, the very strong acid site peak at 86 ppm remained, even after adsorbing 50 mol% TMPO. The three peaks attributable to unreacted TMPO (42 ppm) and reacted TMPO with single [$TaMoO_6$] sheets (67 ppm) or double [$TaMoO_6$] sheets (86 ppm) were all present for 50 mol% TMPO-adsorbed $HTaMoO_6$ nanosheets. This indicates that most of the aggregated nanosheets consisted of individual sheets, which adsorb only the monolayer of TMPO observed as the main peak at 67 ppm in the ^{31}P NMR spectrum. However, some of the aggregated nanosheets interacted with nearby nanosheets, embracing TMPO like the layered oxide did, which was observable as a peak at 86 ppm in the NMR spectrum.

3.4. Acid catalytic activity

Before examining the acid catalytic activity of both layered and nanosheet $HTaMoO_6$, an intercalation test using benzyl alcohol and sucrose onto $HTaMoO_6$ was performed in isolation by immersing 0.2 g of $HTaMoO_6{\cdot}nH_2O$ (n = 1.35) in 3 mL benzyl alcohol solution or in 5 mL aqueous solution containing 1 g of sucrose under constant shaking for 30 min. The XRD pattern of the resultant material after drying at room temperature is shown in Fig. 6. Immersion in benzyl alcohol shifted the (0 0 1) peaks of both samples to lower angles, corresponding to an increase in basal spacing from 13.6 to 23.6 Å (layered) and 13.9 to 23.8 Å (nanosheet) [31,32]. This shift confirmed the intercalation of benzyl alcohol into the $HTaMoO_6$. Given the interlayer spacing of the fully dehydrated sample (10.8 Å), the total expansion was estimated to be 12.8 Å for layered $HTaMoO_6$ and 13.0 Å for $HTaMoO_6$ nanosheets. Different intercalation peaks were observed for the sucrose solution. The layered $HTaMoO_6$ formed a broad peak at 18.2 Å, and aggregated nanosheets formed a very broad peak at 19.3 Å. Although aggregated $HTaMoO_6$ nanosheets partly involved a layered structure, as shown in Fig. 2, the interlayer space formed by restacking was not uniform, and differed from the original layered oxide. Substrates such as alcohols and sugars are intercalated by the interaction of OH groups of the substrate with strong acid sites in the interlayer of the oxide. The intercalation behavior of sucrose, which possesses many hydroxyl groups, seems more complex, resulting in the formation of layers with different interlayer spacing.

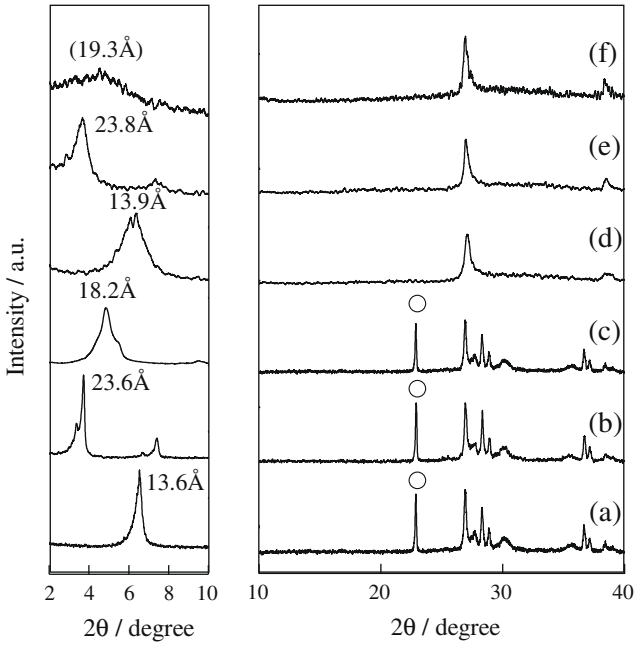

Fig. 6. XRD patterns for (a) layered $HTaMoO_6{\cdot}nH_2O$ (n = 1.35), (b) layered $HTaMoO_6$ after immersion in benzyl alcohol for 30 min, (c) layered $HTaMoO_6$ after immersion in aqueous sucrose solution for 30 min, (d) $HTaMoO_6$ nanosheet aggregate, (e) $HTaMoO_6$ nanosheet aggregate after immersion in benzyl alcohol for 30 min, and (f) $HTaMoO_6$ nanosheet aggregate after immersion in aqueous sucrose solution for 30 min. (○ = $LiTaO_3$ as impurity).

The results for the Friedel–Crafts alkylation of anisole and toluene in the presence of benzyl alcohol using the present catalysts are listed in Table 1. Both layered and aggregated nanosheets of the metal oxides exhibited high activity for the reactions, comparable to layered $HNbMoO_6$ and exceeding the activities of other tested solid acids. Although the difference in performance between layered and nanosheet $HTaMoO_6$ could not be clearly defined for the alkylation of anisole, due to rapid reaction completion within 30 min, a considerable difference was observed for the Friedel–Crafts alkylation of toluene, in which the turnover rate of $HTaMoO_6$ nanosheets was approximately 2.5 times that of layered $HTaMoO_6$.

The results of esterification of acetic acid and lactic acid and the hydrolysis of sucrose and cellobiose over several solid acid catalysts are summarized in Tables 2 and 3. Aggregated $HTaMoO_6$ nanosheets exhibited a high turnover frequency for esterification of both acetic acid and lactic acid, exceeding the turnover frequency of layered $HTaMoO_6$, layered $HNbMoO_6$, and Amberlyst-15 and was comparable to Nafion NR50 for esterification of lactic acid. The turnover frequencies obtained for both layered $HNbMoO_6$ and layered $HTaMoO_6$ were similar for the esterification of acetic acid and lactic acid, and the order of activity corresponded to the results obtained by ^{31}P NMR (86 ppm for layered $HNbMoO_6$ [28] and 85 ppm for layered $HTaMoO_6$) and NH_3-TPD (640 K for layered $HNbMoO_6$ and 678 K for layered $HTaMoO_6$), with only a small difference in acid strength.

Table 1
Friedel–Crafts alkylation of anisole and toluene over several solid acid catalysts.

Catalyst	S_{BET} ($m^2\ g^{-1}$)	Acid amount (mmol g^{-1})	Alkylation of anisole[a]		Alkylation of toluene[b]	
			Yield (%)	TOF (h^{-1})	Yield (%)	TOF (h^{-1})
Layered $HTaMoO_6$	1	1.25[d]	92.2[f]	73.8	38.1	3.8
$HTaMoO_6$ nanosheets	23	1.00[d]	88.7[f]	88.7	77.2	9.7
Layered $HNbMoO_6$	5	1.85[d]	99.0[f]	89.0	74.1	4.9
H-beta[c]	420	1.0[e]	36.6	45.8	0.4	0.1
Amberlyst-15	50	4.8[e]	57.9	3.0	14.0	0.4
Nafion NR50	<0.1	0.9[e]	62.5	17.4	19.0	2.6

[a] Reaction conditions: anisole (100 mmol), benzyl alcohol (10 mmol), catalyst (0.2 g), 373 K, 2 h.
[b] Reaction conditions: toluene (100 mmol), benzyl alcohol (10 mmol), catalyst (0.2 g), 353 K, 4 h.
[c] SiO_2/Al_2O_3 = 25, JRC-Z-HB25.
[d] Determined by ^{31}P NMR.
[e] Refs. [38–41].
[f] Reaction time 30 min. N.D. – not detected.

Table 2
Esterifications of acetic acid and lactic acid catalyzed by several solid acid catalysts.

Catalysts	Acid amount (mmol g^{-1})	Esterification of acetic acid[a]		Esterification of lactic acid[b]	
		Reaction rate (mmol g^{-1} min^{-1})	TOF (h^{-1})	Reaction rate (mmol g^{-1} min^{-1})	TOF (h^{-1})
Layered $HTaMoO_6$	1.25[c]	0.09	4.3	0.26	12.3
$HTaMoO_6$ nanosheets	1.00[c]	0.28	17.0	0.43	25.9
Layered $HNbMoO_6$	1.85[c]	0.17	5.5	0.48	15.6
Amberlyst-15	4.8[d]	0.89	11.7	0.54	6.7
Nafion NR50	0.9[d]	0.44	29.2	0.38	25.6

[a] Reaction conditions: ethanol (1 mol), acetic acid (0.1 mol), catalyst (0.2 g), 343 K, 4 h.
[b] Reaction conditions: ethanol (1 mol), lactic acid (0.088 mol), catalyst (0.2 g), 343 K, 2 h.
[c] Determined by ^{31}P NMR.
[d] Refs. [38–41].

Table 3
Hydrolysis of disaccharides over several solid acid catalysts.

Catalysts	Acid amount (mmol g^{-1})	Hydrolysis of sucrose[a]		Hydrolysis of cellobiose[b]	
		Rate of glucose production (mmol g^{-1} h^{-1})	TOF (h^{-1})	Rate of glucose production (mmol g^{-1} h^{-1})	TOF (h^{-1})
Layered $HTaMoO_6$	1.25[d]	18.3	14.6	0.44	0.35
$HTaMoO_6$ nanosheets	1.00[d]	25.1	25.1	0.47	0.47
Layered $HNbMoO_6$	1.85[d]	24.1	13.0	0.31	0.17
$Nb_2O_5{\cdot}nH_2O$	0.3[e]	0.3	1.0	0	0
H-ZSM5[c]	0.2[e]	0.1	0.7	0	0
Amberlyst-15	4.8[e]	6.6	1.4	0.22	0.05
Nafion NR50	0.9[e]	2.2	2.4	0.16	0.18
H_2SO_4	20.4	45.6	2.2	6.73	0.33

[a] Reaction conditions: sucrose (1.0 g, 2.92 mmol), H_2O (20 mL), catalyst (0.2 g), 353 K.
[b] Reaction conditions: cellobiose (1.0 g, 2.92 mmol), H_2O (10 mL), catalyst (0.2 g), 368 K.
[c] SiO_2/Al_2O_3 = 90, JRC-Z-5-90H.
[d] Determined by ^{31}P NMR.
[e] Refs. [38–41].

For hydrolysis of disaccharides (sucrose and cellobiose), both layered and nanosheet $HTaMoO_6$ produced monosaccharide, much more efficiently than conventional solid acids. It should be noted that the catalytic activity of layered $HTaMoO_6$ for hydrolysis of cellobiose was higher than that of layered $HNbMoO_6$ [26] and was comparable to liquid sulfuric acid in terms of turnover frequency. For green chemical transformation, it is strongly required that $HTaMoO_6$ catalysts could be reused for further reactions. The $HTaMoO_6$ was recoverable by filtration and washing with water to remove residue, and the material was confirmed to be reusable with no change in activity (within 5%) after three reuse cycles at hydrolysis of sucrose. Similar to the Friedel–Crafts alkylation and esterification, $HTaMoO_6$ nanosheets had a higher turnover frequency than the layered samples. This difference was most likely caused by the different intercalation abilities of layered $HTaMoO_6$ and $HTaMoO_6$ nanosheets observed using ^{31}P NMR and NH_3-TPD. One possible reason for the higher catalytic activity of $HTaMoO_6$ nanosheets compared to layered oxide was the presence of strong acid sites, formed by the exposure of a single layer (nanosheet), and appearing as a peak at 562 K in the NH_3-TPD. And the layered structure formed by the aggregated single nanosheets with the intercalation availability and strong acid strength (appearing as peaks at 711 K in the NH_3-TPD and 86 ppm for ^{31}P NMR) also contributed to the increased catalytic activity.

4. Conclusions

Layered and nanosheet aggregates of $HTaMoO_6$ were examined as solid acid catalysts for reactions such as Friedel–Crafts alkylation, hydrolysis, and esterification. $HTaMoO_6$ aggregated-nanosheet catalyst was found to function as a strong solid acid catalyst, exceeding the activity of layered $HTaMoO_6$ and $HNbMoO_6$, niobic acid, zeolites, and ion-exchange resins for Friedel–Crafts alkylation of anisole and toluene and hydrolysis of sucrose and cellobiose, and with comparable performance to ion-exchange resins for esterification of acetic acid and lactic acid. NH_3-TPD and ^{31}P MAS NMR measurements indicated that different from previous studied $HNbMoO_6$ nanosheets, $HTaMoO_6$ nanosheets possess additional strong acid sites on the oxide formed by exposure of a single layer, along with strong acid sites within the interlayer of the layered structure of the aggregate, resulting in higher acid catalytic activity than that of the original layered oxide.

Acknowledgments

This work was supported by the Development in a New Interdisciplinary Field Based on Nanotechnology and Materials Science program of the Ministry of Education, Culture, Sports, Science and Technology (MEXT) of Japan and the Global Center of Excellence Program for Chemistry.

References

[1] P.T. Anastas, T C. Williamson (Eds.), Green chemistry: designing chemistry for the environment, American Chemical Society, Washington, DC, 1996, p. 1.
[2] J.H. Clark, Green Chem. 1 (1999) 1.
[3] P. Laszlo, Accounts Chem. Res. 19 (1986) 121.
[4] T.J. Pinnavaia, Science 220 (1983) 365.
[5] T. Kawabata, T. Mizugaki, K. Ebitani, K. Kaneda, J. Am. Chem. Soc. 125 (2003) 10486.
[6] A. Corma, H. García, Chem. Rev. 103 (2003) 4307.
[7] G.J. Kramer, R.A. van Santen, C.A. Emeis, A.K. Nowak, Nature 363 (1993) 529.
[8] R.A. Sheldon, R.S. Downing, Appl. Catal. A: Gen. 189 (1999) 163.
[9] T. Okuhara, N. Mizuno, M. Misono, Adv. Catal. 41 (1996) 113.
[10] A. Corma, A. Martínez, C. Martínez, J. Catal. 164 (1996) 422.
[11] N. Horita, M. Yoshimune, Y. Kamiya, T. Okuhara, Chem. Lett. (2005) 1376.
[12] M. Hino, S. Kobayashi, K. Arata, J. Am. Chem. Soc. 101 (1979) 6439.
[13] K. Ebitani, J. Konishi, H. Hattori, J. Catal. 130 (1991) 257.
[14] B.H. Davis, R.A. Keogh, R. Srinivasan, Catal. Today 20 (1994) 219.
[15] M.A. Harmer, W.E. Farneth, Q. Sun, J. Am. Chem. Soc. 118 (1996) 7708.

[16] M. Hara, T. Yoshida, A. Takagaki, T. Takata, J.N. Kondo, S. Hayashi, K. Domen, Angew. Chem. Int. Ed. 43 (2004) 2955.
[17] M. Toda, A. Takagaki, M. Okamura, J.N. Kondo, K. Domen, S. Hayashi, M. Hara, Nature 438 (2005) 178.
[18] T. Okuhara, Chem. Rev. 102 (2002) 3641.
[19] K. Tanabe, W.F. Hölderich, Appl. Catal. A 181 (1999) 399.
[20] A. Takagaki, M. Sugisawa, D. Lu, J.N. Kondo, M. Hara, K. Domen, S. Hayashi, J. Am. Chem. Soc. 125 (2003) 5479.
[21] A. Takagaki, T. Yoshida, D. Lu, J.N. Kondo, M. Hara, K. Domen, S. Hayashi, J. Phys. Chem. B 108 (2004) 11549.
[22] A. Takagaki, D. Lu, J.N. Kondo, M. Hara, S. Hayashi, K. Domen, Chem. Mater. 17 (2005) 2487.
[23] A.S. Dias, S. Lima, D. Carriazo, V. Rives, M. Pillinger, A. A Valente, J. Catal. 244 (2006) 230.
[24] C. Tagusagawa, A. Takagaki, S. Hayashi, K. Domen, J. Phys. Chem. C 113 (2009) 7831.
[25] C. Tagusagawa, A. Takagaki, S. Hayashi, K. Domen, J. Am. Chem. Soc. 130 (2008) 7230.
[26] A. Takagaki, C. Tagusagawa, K. Domen, Chem. Commun. (2008) 5363.
[27] A. Takagaki, R. Sasaki, C. Tagusagawa, K. Domen, Top. Catal. 52 (2009) 592.
[28] C. Tagusagawa, A. Takagaki, S. Hayashi, K. Domen, Catal. Today 142 (2009) 267.
[29] G. Blasse, A.D.M. de Pauw, J. Inorg. Nucl. Chem. 32 (1970) 3960.
[30] J.L. Fourquet, A. Le Bail, P.A. Gillet, Mater. Res. Bull. 23 (1988) 1163.
[31] V. Bhat, J. Gopalakrishnan, Solid State Ionics 26 (1988) 25.
[32] N.S.P. Bhuvanesh, B.R. Prasad, C.K. Subramanian, J. Gopalakrishnan, Chem. Commun. (1996) 289.
[33] N. Kinomura, N. Kumada, Solid State Ionics 51 (1992) 1.
[34] R.E. Shaak, T.E. Mallouk, Chem. Commun. (2002) 706.
[35] E.F. Rakiewicz, A.W. Peters, R.F. Wormsbecher, J. Phys. Chem. B 102 (1998) 2890.
[36] H.M. Kao, C.Y. Yu, M.C. Yeh, Micropor. Mesopor. Mater. 53 (2002) 1.
[37] Q. Zhao, W.H. Chen, S.J. Huang, Y.C. Wu, H.K. Lee, S.B. Liu, J. Phys. Chem. B 106 (2002) 4462.
[38] K. Tanabe, Mater. Chem. Phys. 17 (1987) 217.
[39] K. Tanabe, S. Okazaki, Appl. Catal. A: Gen. 133 (1995) 191.
[40] M.A. Harmer, Q. Sun, Appl. Catal. A: Gen. 221 (2001) 45.
[41] H. Matsuhashi, K. Arata, Phys. Chem. Chem. Phys. 6 (2004) 2529.